Journal of Non-Newtonian Fluid Mechanics 319 (2023) 105071

Contents lists available at ScienceDirect

Journal of Non-Newtonian Fluid Mechanics

journal homepage: www.elsevier.com/locate/jnnfm

Shear-induced particle migration in a cement slurry under oscillatory pipe flow

Valmir Kabashi, Teresa Liberto, Agathe Robisson *

Institute of Materials Technology, Building Physics and Construction Ecology, Faculty of Civil and Environmental Engineering, TU Wien, Karlsplatz 13, 1040 Vienna, Austria

ARTICLE INFO

Keywords:
Particle migration
Cement
Blockage
Yield stress fluid
Thixotropic fluid
SAOS

ABSTRACT

The behavior of a suspension of spherical particles in a yield stress, shear thinning, thixotropic fluid is studied under pipe flow at low Reynolds number. Three flow distances, imposed by large amplitude oscillations, are investigated: 25 m, 48 m and 200 m, below and above the development length predicted for a Newtonian suspension of identical bead size and pipe diameter. The base fluid is a cement slurry and the particles are red glass beads, added at 0.3 vol. fraction (ϕ_0).

The radial distribution of beads over the pipe cross-section is measured after the hardening of the cement and shows a concentration gradient. No clear influence of travel distance is observed. Averaging all results, an increase in bead concentration by 35% above ϕ_0 (reaching an average $\phi = 0.41$) is measured in the pipe center region, and a decrease by 20% (reaching an average $\phi = 0.24$) near the pipe wall. The absence of further densification of beads in the pipe center contrasts with results obtained in Newtonian fluids. This is attributed to the paste increase in yield stress with time at rest, predicted to result in a plug flow zone of increasing radius with time.

The radial migration of particles evidenced in this work for a low yield stress cement slurry may contribute to the formation of plugs (zone of high concentration of aggregates) observed at the forefront of concrete during pumping, explaining blockage.

1. Introduction

The relative ease of pumping concrete through pipes has been associated with the formation of a lubricating layer, sometimes called boundary layer, that develops near the pipe wall during pumping and where the shear concentrates [1,2]. This lubricating layer has been defined as a layer of fluid mixture where the shear rate is high and that contains a lower portion of large (≈ cm-size) particles than the bulk concrete. Its existence was experimentally confirmed in pumped concrete by ultra-sonic measurements and optical micrography, and its thickness was shown to be approximately 2 mm (in pipes of internal diameter 100–125 mm), depending on the initial particle concentration in the concrete [1,3,4]. Ngo and co-authors [5] developed a shearing device that allowed to collect the mixture constituting the lubricating layer. They tested concrete mixes containing aggregates ranging from micrometers to 40 mm and showed that the collected mixture contained only particles smaller than 0.25 mm. The formation of this layer has been attributed to shear induced migration that contributed to particle volume fraction heterogeneities beyond the geometric wall effect [1,4,6,7].

While the migration of aggregates away from the wall has been shown to be beneficial to reduce pumping pressure, their more central position in the pipe results in their increased velocity, which may in turn drive their accumulation at the concrete front and cause flow blockage . Such particle accumulation at the interface between the front of a flowing suspension (advancing meniscus) and air has been evidenced in Newtonian based fluid suspensions under pipe flow [8] and under squeezing flow [9]. In fresh concrete, blockage during priming (i.e., the process during which the pipes are being filled with concrete) dominates pumping failure occurrences [10] but remains a poorly understood phenomenon [6]. Failure was identified to be linked to concrete “dewatering” or “desaturation” where the interparticle space is not filled with fluid and the flow becomes frictional [11]. Therefore, while the migration of aggregates away from the wall at distances of millimeters has been linked to lower than expected pumping pressures, their migration further away from the wall, and towards the center of the pipe, may be linked to pumping blockage. This phenomenon, which, to our knowledge, has not been experimentally shown in concretes or other suspensions of cementitious slurries, motivated the present work.

* Corresponding author.
E-mail address: agathe.robisson@tuwien.ac.at (A. Robisson).

https://doi.org/10.1016/j.jnnfm.2023.105071
Received 18 January 2023; Received in revised form 16 May 2023; Accepted 20 May 2023
Available online 26 May 2023

Numerous studies have addressed particle migration in Newtonian, generalized Newtonian, or viscoelastic fluids. Suspensions made with non-Brownian particles can indeed experience de-mixing when sheared under heterogeneous shear stress field, as in pipe flow. This effect was first observed by Gadala-Maria and Acrivos in 1980 [12]. In this study, a suspension of silicone oil and polystyrene particles of diameter 40–50 μm was sheared in a Couette rheometer at a constant angular velocity, and a drift in the torque was measured over time (i.e., hours). Leighton and Acrivos [13] later explained that this decrease in torque was due to the particles migrating out of the sheared Couette gap into the fluid reservoir below the bob, where the suspension experienced lower shear rates.

In laminar pipe flow, particle migration was first studied in Newtonian base fluids using MRI [14,15] and optical tools [16,17]. Authors demonstrated the migration of particles away from the wall, where the shear gradient is high, and towards the center of the pipe, where the shear gradient is low. For example, Koh and Leal [14] studied suspensions prepared with initial solid volume fractions of particles ϕ_0 of 0.1, 0.2 and 0.3 in a rectangular channel with a particle radius to channel width ratio of 0.019. They measured the development of concentration gradients in all cases, with maximum concentrations in the center of the channel equal to 0.2, 0.51 and 0.64 (i.e., near close random packing), for the suspensions of initial ϕ_0 of 0.1, 0.2 and 0.3, respectively. They also showed that the migration is accompanied by a blunting, or flattening, of the particle velocity profile.

Shear-induced migration is mostly due to hydrodynamic interactions that gradually drive the motion of particles to zones of lower shear [18], and can occur at zero Reynolds number. This phenomenon is to be distinguished from the migration occurring in dilute suspensions, evidenced by Segre and Silberberg [19,20], where particles migrate to an equilibrium position at a radius of about 0.6 R, (with R being the pipe radius), at a relatively small (but not ignorable) Reynolds number.

Particle migration to the pipe center also occurs when the flow is oscillatory and the oscillation amplitude is large enough [21]. Snook, Butler & Guazzelli [22] looked at suspensions based on a Newtonian fluid and particles that matched the refractive index and density of the fluid, with concentrations between 0.1 and 0.4 in volume. They built a large-amplitude oscillatory flow setup to study the dynamics of the shear-induced migration process while maintaining a static optical system and confirmed that the behavior of the suspension was similar to its behavior under unidirectional pipe flow.

Suspensions with non-Newtonian base fluids have also been studied, confirming the phenomenon of particle shear-induced migration in these more complex fluids [23,24]. In shear-thinning fluids, other effects come into play. Huang & Joseph [25] have shown with numerical simulations at moderate Reynolds numbers and $\phi_0 = 0.21$ (in 2D) that shear thinning causes some particles to migrate away from the channel center towards the wall. Similar results were observed in shear-thinning viscoelastic fluids [26]. Comparing Newtonian, shear-thinning and shear-thickening fluids through computations, Martys and co-authors [24] showed that the shear-thinning fluid experienced the most blunted velocity profile, stemming from the shear localization near the wall in their gravity driven flow. They called it an apparent slip effect even though a strict no slip boundary condition was imposed in the simulations.

For a description of the current modeling approaches capturing shear-induced particle migration in Newtonian and non-Newtonian fluids, we refer the reader to the work of Leighton & Acrivos (diffusion model) [13], Nott & Brady (suspension balance model where normal stresses arise from hydrodynamic interactions due to the presence of particles) [18], as well as Morris & Boulay [27], Snook et al. [22], and for non-Newtonian effects, Izadi & Frigaard [28], Hormozi & Frigaard [29], Siqueira & de Souza Mendes [30], and finally D'Avino et al. [31] for viscoelastic (second-order) suspending fluids. The measurement of the normal stresses arising from the presence of particles has been performed using flush-mounted differential pressure transducers installed on the lower parallel plate [32] or on the outer cup of a cylindrical Taylor–Couette cell [33] as well as using a customized plate-plate geometry with imposed particle pressure [34,35].

Fresh cement paste can be considered a fluid of extreme complexity, and, being the subject of the present study, the microstructural origins of its rheological behavior are described next. Cement slurry is prepared by mixing unreacted cement particles (ground clinker, size ≈10 μm) and water (plus additives in most industrial applications). As soon as the particles are put in contact with water, a dissolution-precipitation process starts, raising the pH of the solution to ≈12 in a few seconds [36]. The resulting fluid is a paste that exhibits colloidal behavior due to the nano-particles of calcium silicate hydrates (C-S-H) [37,38] that precipitate on the surface of the cement grains and interact with each other and with the highly surface charged cement particles through an interstitial solution of high ionic strength [39,40]. In a matter of seconds, the ground clinker particles and nano-hydrates will form a strongly cohesive network that will further build up with time at rest [41–43], giving rise to the macroscopic yield stress of cement (and concrete) [44–46]. At rest, i.e., in quiescent conditions, the yield stress increases with time. Upon flow, this multiscale network (micron-size-cement and nano-size-C-S-H particles) is broken down (fluidized) and the slurry flows [47]. This process appears, macroscopically, reversible over a time frame of ≈1 h and gives rise to the so-called thixotropic properties of cement. The dissolution-precipitation process happens continuously over time until most of the cement clinker has reacted (provided enough water is present), the paste having long transitioned into a hard solid by that time.

The interactions described above are so strong that it is typically difficult to prepare a mixture from cement and water below a water-to-cement ratio (w/c) of 0.3 (corresponding to ϕ_0 ≈0.52). To reduce particle interactions (i.e., reduce the yield stress), superplasticizers (SP) can be used. These typically long organic polymeric chains adsorb on the surface of newly precipitated hydrates, and reduce the strong attraction between (charged C-S-H/cement) particles [48]. The resulting low yield stress concretes are called self-compacting concretes (SCC) due to their property of self-leveling placement (they do not require vibration to flow, unlike conventional concretes).

In this work, the study fluid, a cement slurry, was prepared with (white) ordinary Portland cement, water and a superplasticizer. It was combined with (red) spherical glass beads that replaced the irregularly shaped sand grains typically used in conventional mortars, and is representative of the matrix of a self-compacting concrete. The absence of large aggregates enables us to reduce the size of the experimental setup (pipe diameter of 16 mm) and perform an extensive rheological characterization in a conventional (regular size cup) rheometer. The work focuses on capturing the radial migration of beads when the mortar is pumped in a pipe, beyond the mm-scale migration discussed in literature. To document particle migration over long pumping distances, a large amplitude oscillatory flow setup was built. Unlike suspensions cited above where index match enabled the use of optical tools to visualize migration, cement is non transparent and the quantification was performed on hardened, cut and polished cement cores, using the contrast between the white cement matrix and the red beads.

This paper is organized as follows. Section 2 starts with the description of the materials, preparation and characterization method (i.e., rheology) and continues with the description of the setup and pumping protocol, along with the rationale behind the choice of flow distances. The theoretical models used to calculate the velocity profiles are also presented. Section 3 shows the extensive rheological characterization of the slurry, the image analysis of the core, the quantification of bead radial concentration and offers a discussion that proposes a interpretation for the results. A conclusion and perspectives end the article.

2. Materials and methods

2.1. Materials and mixing process

White cement (CEM I 52.5 N, Danucem, $\rho \simeq 3.1$ g cm^{-3}) was used together with spherical red beads (Kugel Pompel, $\rho \simeq 2.5$ g cm^{-3}) to ensure high contrast between the particles (beads) and the matrix (cement slurry) and facilitate the image analysis. The bead particle size distribution was measured with a laser diffraction particle size analyzer (Mastersizer 3000 Malvern), showing D10 = 360 μm, D50 = 470 μm, and D90 = 620 μm. The cement slurry was formulated with a water-to-cement ratio (w/c) of 0.35, 0.80% by weight of cement (bwoc) of a polycarboxylether (PCE)-based superplasticizer (ACE 430, BASF, $\rho = 1.06$ g cm^{-3}) and 0.39% bwoc of retarder (SikaTard®-930, Sika, $\rho = 1.10$ g cm^{-3}). The amount of superplasticizer was optimized to obtain a cement slurry with a dynamic yield stress of approximately 20 Pa. The retarder was added to help maintain the rheological properties constant over the time of the experiment. The resulting fluid, i.e., the cement slurry, although a suspension in itself, is treated as a continuum. Its density was calculated from composition and is equal to 2 g cm^{-3}. Finally, beads were added to the cement slurry at a targeted solid volume fraction $\phi_0 = 0.3$. The 20 Pa yield stress is sufficient to suspend the glass beads in the slurry under quiescent conditions, despite the density difference [49].

The same quantity of slurry (800 mL) was prepared for each experiment following the exact same protocol, using an overhead stirrer (IKA STARVISC-200). The rheological properties of cement slurries being dependent on the mixing protocol and the quantity of slurry mixed [50,51], reproducibility errors were therefore minimized. First, distilled water, PCE and retarder were gently mixed (100 rpm) for 30 s. Then, cement was slowly added and mixed at an increasing velocity (100 to 800 rpm) during two minutes. Glass beads were eventually added to the homogeneous paste until a visually uniform distribution (red color) was observed (less than 1 min). The mixer was then stopped, the slurry scraped from the container wall and remixed for additional 30 s at the maximum speed (800 rpm). The obtained mortar was then left to rest for 10 min and finally stirred for an additional minute at maximum velocity. This procedure was followed after a preliminary study showed that the yield stress of the fresh mortar reached a plateau after a 10 min rest and re-mix, leading to a fairly constant rheological behavior over the experimental time. Note that the complete rheological characterization was performed in the presence of beads as their presence during mixing was observed to modify the rheology of the cement matrix.

2.2. Rheological characterization

Fresh cements, and by extension fresh mortars, typically exhibit a viscosity that varies with shear rate (they are shear thinning and/or shear thickening), are thixotropic (their viscosity varies with the flow history) and have a yield stress (they behave like a viscoelastic solid below their yield stress and like a fluid above) [52–55]. Their properties strongly evolve over time (i.e., structuration buildup) and with temperature [56–58]. These rheological characteristics are crucial to determine the velocity profile, and in particular the yielded regions, of the mortar flowing in the pipe, which in turns dictates the region where shear-induced particle migration can occur [30,59]. This explains the extensive rheological characterization performed in this study and described below.

A stress-controlled rheometer (Anton Paar MCR 302) was used with a vane geometry and a sand blasted cup (Anton Paar ST22-4V-16 + CC27S). This geometry was chosen to maximize the volume of sheared slurry within the cup [60,61]. A lid was always used to minimize sample drying. Tests were performed at 20 °C to represent room temperature and at 35 °C to represent the mortar upon heating during pipe flow. The mortar characterization described below includes (1) flow curves and dynamic yield stress measurement (2) structuration and static yield stress measurement, both over time and at two temperatures.

Flow ramp for dynamic yield stress measurement. A portion of the mortar (from the original 800 mL batch prepared with the mixing procedure described in Section 2.1) was characterized under flow (i.e., imposed rotational velocity).

The **flow protocol** (Fig. 1, up) consists in an initial pre-shear (PS) of 120 s at 300 s^{-1} to fluidize the mortar, followed by a descending shear rate ramp from 100 to 0.01 s^{-1} (i.e., ramp down) and a subsequent ascending shear rate ramp from 0.01 to 100 s^{-1} (ramp up). Overall, the entire duration of the ramp flow curve was kept as short as possible (240 s) in order to minimize the structuration of the paste that inevitably occurs at low shear rates and results in a hysteresis loop during the ramp-down-and-up measurement [62,63].

To capture the power-law-yield-stress behavior of the mortar, a Herschel-Bulkley (HB) model $\tau = \tau_0 + k \cdot \dot{\gamma}^n$ (for $\tau > \tau_0$), where τ_0 is the *dynamic* yield stress, k the consistency index and n the exponent of the power law, was chosen. The descending flow curve was fitted using Origin with a Levenberg–Marquardt algorithm to minimize the residual. The curve fitting was performed between the shear rate ($\dot{\gamma}$) corresponding to the minimum shear stress (τ) reached, and a maximum $\dot{\gamma}$ covering ca. two orders of magnitude, and resulting in an optimal HB fit (i.e., $R^2 \sim 1$). Fig. 2 shows a typical curve and the fitted HB model.

Structuration and static yield stress measurement. Similarly to the previous test, a portion of the mortar was used to characterize the paste "at rest" (i.e., under small amplitude oscillatory strain or SAOS) and capture both its structuration (progression of its elastic modulus) and the evolution of its *static* yield stress over time.

The **structuration protocol** (Fig. 1, bottom) is composed of a series of successive amplitude sweep (AS) and time structuration (TS) steps. The TS step consists in imposing a constant strain amplitude of $\gamma = 10^{-5}$ to the mortar at a fixed frequency of f = 1 Hz. This maintains the paste within its linear viscoelastic (LVE) regime [43]. The AS step consists in imposing a strain amplitude logarithmically increasing with time, starting from 10^{-5} until the storage modulus G' starts to drop, defining the end of the LVE. The linear elastic modulus G'_{lin} is calculated from the average of the G' plateau values in the LVE. The critical strain amplitude γ_{cr} is defined as the strain amplitude at which the elastic modulus G' drops by 20% from the LVE plateau value [43]. AS and TS steps are applied successively and last respectively 1 to 2 min (depending on the deformability of the mortar) and 5 min (Fig. 1, bottom). The entire test has a duration of about 25 min, corresponding to the approximate duration of the pumping experiment.

From the AS step (i.e., G' vs γ), the *static* yield stress was calculated as $\tau_s = G'_{lin} \cdot \gamma_{cr}$. Microscopically, τ_s represents the stress necessary to detach the first neighboring particles in the gel paste without breaking down its microstructure [43,46,64–66].

Effect of temperature on the behavior of the mortar. The two protocols described above (Fig. 1) were performed at both 20 °C and 35 °C. The latter temperature was reached by heating the sample directly in the rheometer. Immediately after loading the sample in the rheometer cup, a thermocouple (VWR Traceable digital thermometer, with an accuracy of ±0.05 °C) was inserted in the cup and used to manually stir the slurry. About 5 min were necessary to reach the temperature of 35 ± 1°C. After the temperature was reached, the vane geometry was inserted in the cup and the measurement started.

The rheological characterization of the cement slurry was performed at 35 °C to capture the fluid behavior upon experiencing a temperature increase while flowing in the pipe due to viscous dissipation. Temperature increase is known to accelerate the hydration reactions and amplify the paste yield stress increase over time [56–58].

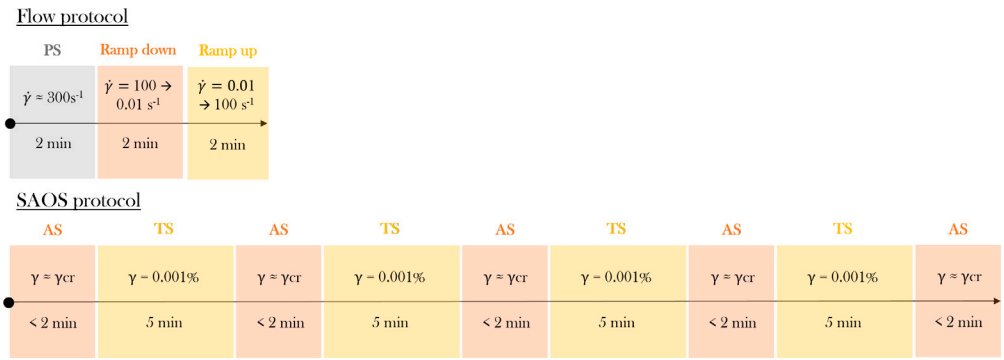

Fig. 1. Rheological characterization: sketch of flow and structuration (SAOS) protocols.

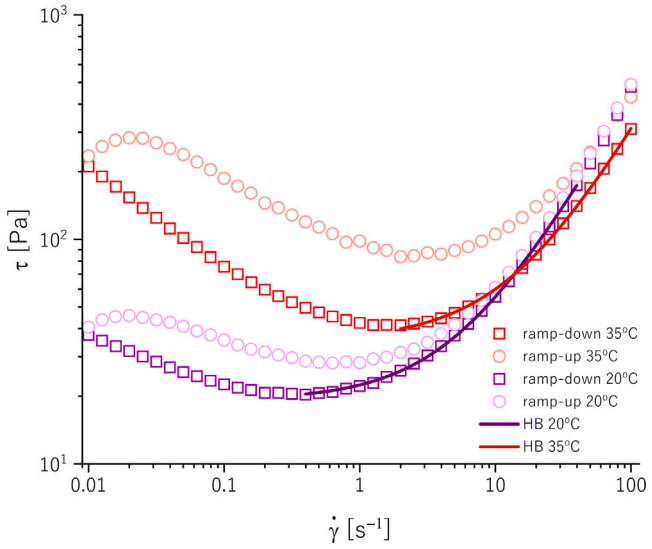

Fig. 2. Representative flow curves (shear stress τ as a function of shear rate $\dot{\gamma}$) obtained on the mortar at 20 °C and 35 °C. Bold violet and red curves (□) were acquired during ramp-down and used for the model identification. Light violet and red curves (○) correspond to the ramp-up and show the hysteresis linked to the structuration of the paste with time. Solid lines (bold violet and red at 20 °C and 35 °C respectively) are the fitted Herschel-Bulkley model covering ca. two orders of magnitude.

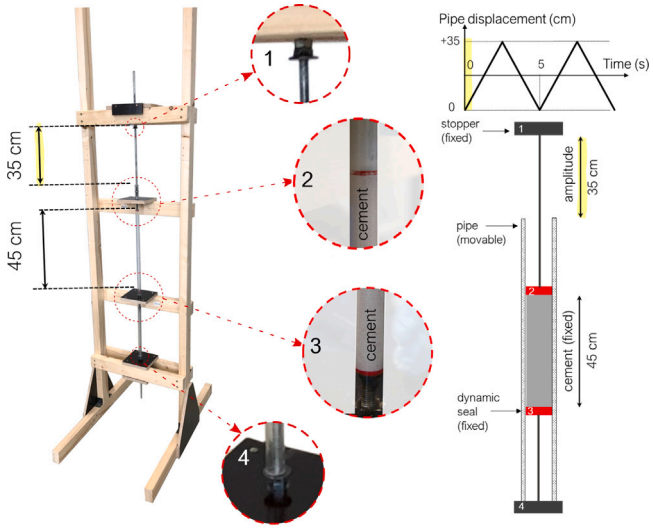

Fig. 3. Customized set-up of oscillatory flow pumping of cement mortar. It is composed of 2 static shafts equipped with dynamic seals (visible in 2 & 3) and a 1 m-long plexiglas pipe that was moved up and down to achieve final flow distance. The applied triangle wave oscillation is schematically plotted.

2.3. Setup oscillatory flow and experimental pumping protocol

Setup. To be able to cover large distances of straight pipe flow and inspired by the works of Snook, Butler & Guazzelli [22], and Mechtcherine, Nerella & Kasten [2], a customized oscillatory pumping setup was built (Fig. 3). A Plexiglas pipe of internal diameter 2 R of 16 mm was selected to obtain a pipe to D50 particle size (radius a) ratio of $R/a = 34$. Wood beams and plates held the Plexiglass pipe while allowing it to move back and forth vertically. Two shafts, acting as pistons, were equipped with dynamic double seals (sourced from HydraulikDichtungen) in their end to prevent leakage of the cement mortar (5 and 6 in Fig. 3). Both shafts were fixed to the wood frame. The distance between the two dynamic seals was about 45 cm (giving the length of the cement core) and the 1 m long plastic pipe could translate up and down by 35 cm, i.e., stroke length $L_i = 35$ cm. This results in an equivalent traveling distance of 70 cm per cycle and a ratio of amplitude of oscillation to pipe diameter $L_i/2R \approx 22$, close to the ratio of 28 used by Snook et al. [22]. At this large amplitude of oscillation, migration towards the center of the pipe has been shown to be similar to the migration observed during steady pumping [21]. Note that this setup is different from the setup of Snook et al., as here, the suspension remains in the same location while the pipe itself is moved back and forth.

Flow distance. Suspensions need to travel a certain distance in a pipe, called the development length, for particles to reach their steady state position after shear-induced radial migration [18]. In Nott & Brady's model, where the base fluid is Newtonian and the particles monodisperse, the distance to achieve steady-state is shown to scale as H^3/a^2, with H being the channel width and a the radius of the particle. Although our suspension is neither Newtonian nor exactly monodisperse, and our flow is oscillatory, we used this model, neglecting the prefactor, to estimate the development length of the glass bead filled cement slurries described here. Using a channel width 2 R of 16 mm and a bead radius of 235 μm, the development length was estimated to be 74 m. Using this result, the travel distances for the suspension were chosen below and above this value to reach 25, 48 and 200 m, in three different experiments.

Oscillatory flow protocol. Before filling the pipe with mortar, it was translated to its bottom position and the upper shaft (equipped with a seal) removed. About 90 mL slurry, prepared following the protocol described in Section 2.1, was then poured into the pipe (Fig. 4) and

Fig. 4. Suspension (cement slurry with beads) while being poured in the pipe.

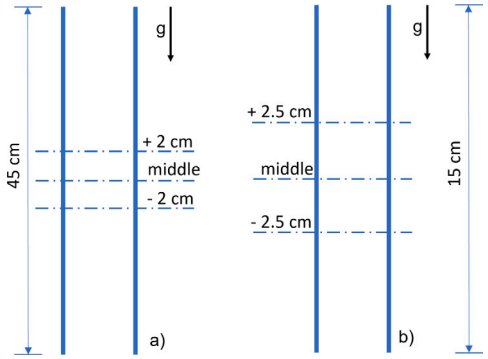

Fig. 5. Schematic of cores and cutting locations in (a) sheared sample and (b) quiescent sample. Each section was polished and photographed for image analysis.

the piston carefully put back into place. Small holes near the top of the pipe, just above the piston, were cut to allow the removal of the air and the surplus mortar, ensuring that the pipe is completely filled with mortar.

In parallel, a pipe of same radius and length of about 15 cm was also positioned vertically with its bottom sealed, filled with the mortar, and left to harden with no further shear applied. This constituted the reference sample (no flow) and was used to draw the baseline of particle radial distribution in the pipe.

Once the filling sequence was achieved, the pumping could start. It was achieved by manually moving the pipe up and down, as steadily as possible, achieving a nearly triangle wave oscillation (Fig. 3). One cycle (up and down movement) covered 70 cm of mortar travel distance and was achieved in an average time of 5 s, giving an average fluid velocity of ≈14 cm/s. This velocity is in the range of velocities typically investigated in concrete (5 to 50 cm/s in [11], 0.5 m/s in [10], 0.3 m/s in [7]) and allowed us to perform the longest test (200 m) in about 25 min.

The particle Reynolds number, defined as $R_{ep} = \frac{U_{max} \cdot \rho . a}{\mu}$ with U_{max} the maximum velocity (approximated to twice the average velocity), ρ and μ the density and the viscosity of the suspending fluid respectively (2 g cm^{-3} and 4.55 Pa·s at 70 s^{-1}, the calculated wall shear rate for a Newtonian fluid), and a the particle radius [14], was calculated to be 0.029. The channel Reynolds number R_e, defined as $R_e = \frac{R_{ep}}{k}$ with k the particle size to pipe diameter ratio (0.03) was calculated to be 0.96. This confirms the laminar regime of the pumped mortar, as most often the case for pumped concrete [6].

After a few minutes of up and down movement, temperature increase could be felt, and was estimated to be between 5 and 10 °C above room T (no sensor was placed inside the pipe to avoid disrupting the flow). At this point, the experiment was briefly stopped and wet cool tissues were applied around the pipe to cool it down. Minimizing temperature increase was important to avoid the acceleration of cement hydration which modifies the rheological properties of the slurry (see Section 2.2).

After the total mortar traveling length was achieved, the experiment was stopped and the mortar left to set for at least 3 days. It is assumed that no relative movement of beads occurred during this time. Six samples (pipe filled with hardened mortar) were obtained: 3 reference samples (ref-25 m, ref-48 m and ref-200 m) and 3 flow samples (flow-25 m, flow-48 m and flow-200 m). The flow samples were then cut in 3 (and in one case 4) locations: 0 cm (i.e., middle), (−3 cm, flow-48 m), −2 cm and +2 cm, all far from the pipe ends to avoid end effects in our analysis (Fig. 5). The reference samples (no flow) were cut 2.5 cm above and below the sample middle length (ref-25 m and ref-200 m cores) and additionally cut in the middle for the ref-48 m sample. These sections were polished and photographed with a Canon EOS 80 camera equipped with a Canon 100 mm lens.

Image treatment. The images of each cross-section were analyzed with ImageJ. Before the image binarization was performed, particles with low contrast were individually digitally colored in red. The contrast was particularly low in case of particles dislodged during sample preparation (either cutting or polishing, even though these steps were performed carefully). After the threshold was set on ImageJ and the image converted to black and white, the binary image was carefully compared with the original picture to ensure no bead was missed. In each image, the cross-section was then divided into 7 circular rings of thickness 1 mm and one circle of radius 1 mm in the center, following the axial symmetry (Fig. 6). Each domain was analyzed individually and the solid volume fraction calculated as the area fraction of beads divided by the total surface area of the domain. The bead local solid volume fraction ϕ was then normalized by the total solid volume fraction (ϕ_0) measured over the whole cross-section. We call this value "normalized ϕ" and plot it as ϕ/ϕ_0. The results presented next are averages from the counts performed on 3 cross-sections (or 4 for the 48-m sample where results displayed large variability) for each flow sample, resulting in a total of 10 analyzed flow cross-sections, and 2 cross-sections (or 3 for the 48 m) for each reference (no-flow) sample, resulting in a total of 7 analyzed reference cross-sections.

2.4. Herschel-Bulkley fluid velocity profile calculation

The velocity profile of a Herschel-Bulkley fluid flowing in a circular pipe can be calculated using the rheological parameters τ_0 (*dynamic* yield stress), k (consistency), and n (power-law exponent).

The velocity distribution as a function of radius r can be written as [67,68]:

$u(r) = (\frac{n}{n+1})\,(\frac{\tau_w}{k})^{1-n}\,R\,[(1-\xi)^{\frac{1+n}{n}} - (\frac{r}{R}-\xi)^{\frac{n+1}{n}}]$ for $r > R_P$, with R_P the radius of the plug flow, τ_w is the wall shear stress, R is the pipe radius, and $\xi = \frac{R_P}{R} = \frac{\tau_0}{\tau_w}$

The parameters τ_w and ξ can be identified from the expression of the average velocity U, known from experiment:

$\frac{U_P}{U} = [1 - \frac{2n}{3n+1}(1-\xi) - \frac{2n^2\xi(1-\xi)}{(3n+1)(2n+1)}]^{-1}$ with U_P being the plug velocity

$$U_P = (\frac{n}{n+1})\,(\frac{\tau_w}{k})^{1-n}\,R\,(1-\xi)^{\frac{1+n}{n}}\,[1 - \frac{2n}{3n+1}(1-\xi) - \frac{2n^2\xi(1-\xi)}{(3n+1)(2n+1)}]$$

This calculation can be considered representative of the oscillatory flow performed in this study using three assumptions. First, we have checked that the transition (or entry) length is much smaller than the stroke. For a homogeneous Newtonian fluid, it can be calculated using the particle Reynolds number R_{ep} (calculated earlier and equal to 0.029) [18], and gives a value of order 1 mm, far below the amplitude of 35 cm. Transition lengths have also been estimated for yield stress fluids and have been shown to stay below a pipe radius [69]. Second, it is assumed that the velocity profile reached during the movement of

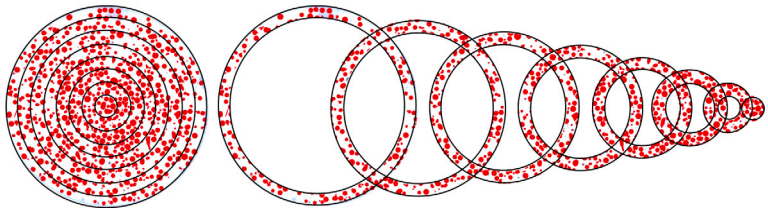

Fig. 6. Picture of a polished cross-section of a sample of hardened cement. The image is divided into 8 axisymmetric domains for image analysis, with the domain boundary visualized by the black circles digitally added to the image.

Table 1
Herschel-Bulkley rheological parameters identified from fitting the flow curves at 20 °C and 35 °C (see Fig. 2) with τ_0, the *dynamic* yield stress, k, the consistency, and n, the power-law exponent.

	T (°C)	τ_0 (Pa)	k ($Pa\ s^{-n}$)	n
HB-20C	20	24.1 ± 5.1	3.4 ± 0.2	1.05 ± 0.02
HB-35C	35	93.8 ± 58.4	2.5 ± 0.2	1.04 ± 0.01

the pipe (flow-boundary motion) is the same as the one reached during a pressure driven flow. This equivalence has often been assumed but it was recently pointed out that this issue requires more attention [70]. Third, we neglect the non-steady rheological properties of the cement (thixotropic characteristics) -in particular its yield stress increase with time at rest-. The development of a model that could capture the flow of a thixotropic fluid under flow produced by an oscillating pipe is beyond the scope of this paper. The velocity profiles plotted for the homogeneous non-reactive cement pastes characterized by rheology are aimed at supporting the discussion.

3. Results and discussion

3.1. Rheology

Dynamic yield stress (τ_0) measurement. The mortar flow curves (Fig. 2) show a typical thixotropic behavior [71]. On the descending flow curve, the value of shear stress reaches a minimum and then rises with further decreasing shear rate (and increasing time) due to the predominant contribution of the paste structuration against the competing shear flow de-structuration. The Herschel-Bulkley model parameters (τ_0, k, and n), calculated from the flow curve fitting between ca. 1 s^{-1} and 100 s^{-1} (Section 2.2), are reported in Table 1 as averages from four sets of parameters identified on 4 tests (20 °C) performed on 4 different mixes, and at times between 0 and 35 min from the initial mixing. These values are considered representative of the slurry during the pumping sequences (that last about 20–30 min) and are used to calculate the velocity profile reported in Section 2.4. The standard deviation shows the modest variation in the properties of the mortar prepared on different days and tested at different times from mixing.

Note that the n exponent is slightly above 1, indicating a fluid that is slightly shear thickening [54,71,72], likely linked to the presence of superplasticizer [73,74].

Structuration and static yield stress (τ_s) measurement. The temporal evolution of τ_s is shown in Fig. 7 (20 °C: purple data points). The evolution of the elastic modulus $G'(t)$ measured in the interval periods and that represents the mortar structuration over time is shown in Appendix. As expected from a cement paste, τ_s increases over time, rising by close to an order of magnitude over 25 min at 20 °C.

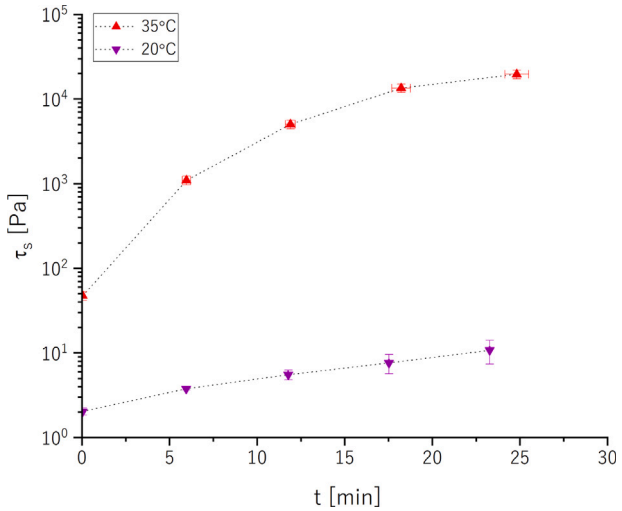

Fig. 7. Static yield stress values (τ_s) obtained by SAOS measurements on the cement mortar (cement slurry with beads) at 20 °C (▽) and 35 °C (△) as a function of time (see protocol in Fig. 1). The error bar is on both x and y axis.

Effect of temperature on the behavior of the mortar. The effect of temperature on both dynamic and static yield stresses is shown in Fig. 2 and Fig. 7, respectively. The flow curves (Fig. 2) show a larger hysteresis at 35 °C than at 20 °C, suggesting a faster structuration of the paste at higher temperature (related to the faster precipitation and aggregation of C-S-H nano-particles), leading to a stronger gel.

The values of the HB model parameters identified at 35 °C are shown in Table 1. They were calculated as an average of two sets of parameters identified on two different tests, performed on two different mixes and at two different times (0 and 25 min at 35 °C). The large standard deviation comes from the rapid evolution of the mortar properties at 35 °C.

The temporal evolution of τ_s at 35 °C (Fig. 7, red data) confirms that the structuration (paste in quiescent conditions) is much faster at 35 °C than at 20 °C. The static yield stress reached a value of $1.5{\cdot}10^3$ Pa after ca. 7 min at 35 °C and rises up to $2{\cdot}10^4$ Pa after ca. 25 min, gaining almost three orders of magnitude after 25 min "at rest" and at 35 °C.

3.2. Pipe velocity profile prediction and size of plug core

Using the theory shown in Section 2.4 and the Herschel-Bulkley models identified on the mortar tested at 20 °C and 35 °C (Table 1), the velocity profiles were calculated (Fig. 8). Also plotted are the velocity profiles of a Newtonian fluid, for reference, and a third model using k and n as in HB-35C and a yield stress τ_s = 1500 Pa (measured after 7 min at 35 °C using SAOS protocol, i.e., *static* yield stress).

The radius of the plug flow region was evaluated to be 0.075 R at 20 °C and 0.28 R at 35 °C, with R the radius of the pipe, or resp. 1.3 and

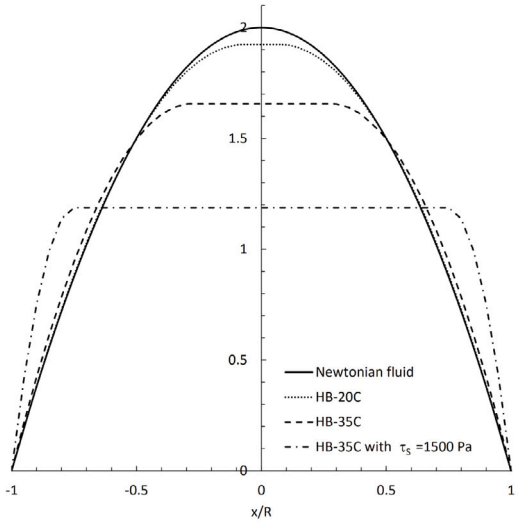

Fig. 8. Velocity profiles calculated for a Newtonian fluid, and for 3 HB fluids following Table 1 and using τ_s = 1500 Pa (Fig. 7), k = 2.5, and n = 1.04.

4.8 particle diameters. Using τ_s=1500 Pa, the radius of the plug flow region is calculated to cover about 0.75 R, or 13 particle diameters.

These profiles show that, at 20 °C, the diameter of the plug flow is negligible, and the fluid is initially predicted to be sheared nearly over the whole section of the pipe diameter, setting the conditions for particle migration. While this profile was calculated considering the fluid homogeneous, i.e., no migration has happened yet, it will, upon migration, get blunted [17,24,75], and, within this blunted region, low shear will occur, setting up the conditions for further paste structuration i.e., fluid local yield stress increase.

3.3. Radial particle distribution in pipe: reference and flow samples

Fig. 9 shows representative cross-sections of four samples coming from the four experiments: no flow, and traveled distances of 25 m, 48 m and 200 m. Visible to the naked eye is a noticeable difference between the reference sample and the flow samples. The latter exhibit a seemingly higher concentration of particles in the center region of the pipe and a lower concentration in the region near the pipe wall.

The average bead nominal concentration on all samples (17 cross-sections in total) was found to be 31.6 ± 1.9%. Note this is slightly above the target concentration (30%), likely due to an overestimation of the glass density (beads may contain air bubbles). The samples showed no dependence of nominal concentration on the vertical position of the examined cross-section, confirming that sedimentation effects can be neglected [49].

The averaged normalized bead contents (ϕ/ϕ_0) plotted as a function of the normalized radial position (r/R) are shown Fig. 10. The error bar represents the standard deviation measured over all available samples (3 to 4 cross-sections for each flow samples, 7 cross-sections for the reference sample). A horizontal line is added at a normalized concentration of 1 to help visualize a perfectly uniform distribution.

The reference sample shows a uniform distribution over the whole pipe cross-section, within the error bar. The error is large towards the center of the pipe, likely due to the small surface area considered. Near the wall, there is a tendency for the bead concentration to drop.

All flow cases exhibit radial variations of bead content over the pipe cross-section, with a higher concentration near the center (25 to 46% higher than the nominal concentration at r/R ≤ 0.2) and lower at the pipe wall (5 to 30% lower than nominal concentration at r/R > 0.9). This is consistent with results obtained in other fluids and discussed in the introduction, where shear-induced particle migration drives particles from high shear (near pipe wall) to low shear rate (pipe center) regions. The low concentration near the pipe wall is not only due to the presence of the wall but is a result of the particle migration towards the pipe center causing depletion of particles at its periphery.

The 25 m flow sample shows a slightly different concentration profile, with a normalized bead content non-uniformly increasing from the pipe wall towards its center. It displays a minimum normalized concentration (≈20% below nominal concentration) not near the wall but closer to the center at 0.5 < r/R < 0.7, and a concentration close to nominal towards the wall (≈3% below nominal concentration at 0.7 < r/R < 1.0). Particle wall attraction, described before in shear thinning fluids [25,26], and that opposes shear-induced migration towards the pipe center, may explain this result. The present mortar, with a power n slightly above 1 (in the shear rate region explored, i.e., below 100 s^{-1}), indicates a slightly shear thickening suspension, rather than shear thinning. Nevertheless, the reduced bead content near the wall locally modifies the rheology (lower bead content will lead to a lower viscosity), and in turn the shear rate, making a definite explanation difficult. This effect is not visible anymore when the mortar is pumped over longer distances (and times). Here, the evolution of the mortar properties over time, i.e., increase of yield stress at rest (especially at 35 °C), may modify the plug core radius and consequently the velocity profile, which could play a role in changing the wall attraction.

Besides this contrast in behavior near the pipe wall, results obtained for the three pumping distances are similar, showing no trend with flow distance. More specifically, further densification of beads towards the pipe center is not observed for longer shear distances, as it is observed for Newtonian fluids. The experimental data obtained from the three experiments (25 m, 48 m and 200 m flow) were then combined to build a unique curve (Fig. 11), showing a normalized concentration ϕ/ϕ_0 of 1.35 at 0 < r/R < 0.2 (pipe center) and of 0.8 at 0.875 < r/R < 1. In contrast, Koh et al. [14] observed that a suspension prepared with a Newtonian fluid and particles at $\phi_0 = 0.3$ would exhibit a particle concentration in the center region of $\phi = 0.64$, or ϕ/ϕ_0=2.13.

We hypothesize that further migration is hindered by the evolution of the cement matrix rheology, and in particular the increase in yield stress with time. Indeed, upon migration of particles to the pipe center and without considering any fluid thixotropy, the velocity profile of a Newtonian fluid is predicted to evolve from a near-parabolic velocity profile to a blunted or (near-)plug flow velocity profile. This blunting was observed experimentally and numerically in Newtonian fluids [14,15,17], shear thinning [25] and shear thickening fluids [24]. Within the (near-)plug flow region, the cement paste is not (or only slightly) sheared, and under these quiescent conditions ("at rest"), will build up its structure, increasing its static yield stress (as shown in Fig. 7). This, in turn, will further increase the radius of the central plug core and move the sheared (i.e. yielded) region closer to the pipe wall. Fig. 8 illustrates this effect: the plug radius covers about 75% of the pipe radius when the yield stress is increased to 1500 Pa (reached in the paste after 7 min at 35 °C). Within this plug region, no shear gradient occurs and consequently no bead migration can take place. In summary, the paste increasing yield stress with time, that results from cement structuration, may explain why further bead compaction does not occur at larger pumping distances in this slurry. Other effects, still debated today, such as the finite particle to pipe size ratio and the dependence of the particle normal stress on the initial particle concentration, may play a role [17,22,76].

4. Conclusion

In this work, we built a rather simple but effective oscillatory flow setup where a circular pipe is used to pump cement mortars composed of white cement and 0.30 vol. fraction red glass beads. Three pumping distances were used, 25, 48 and 200 m, chosen below and above the

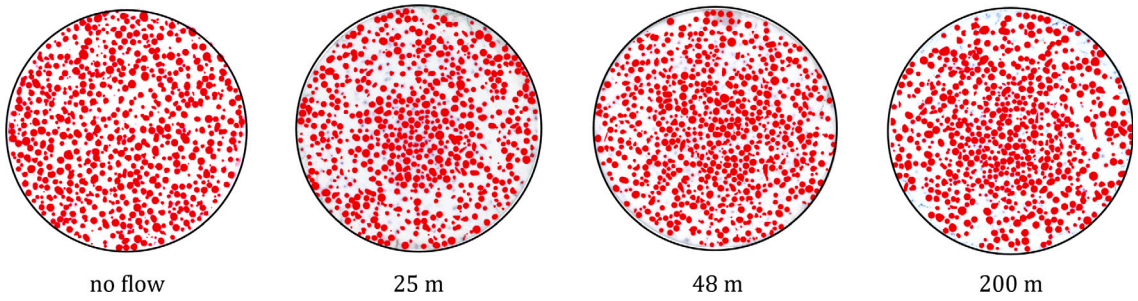

Fig. 9. Representative cross-sections of cut and polished hardened cement samples after no flow (quiescent conditions), and flow with 25 m, 48 m, and 200 m traveled distance. (Bead red color was digitally enhanced for better visualization.).

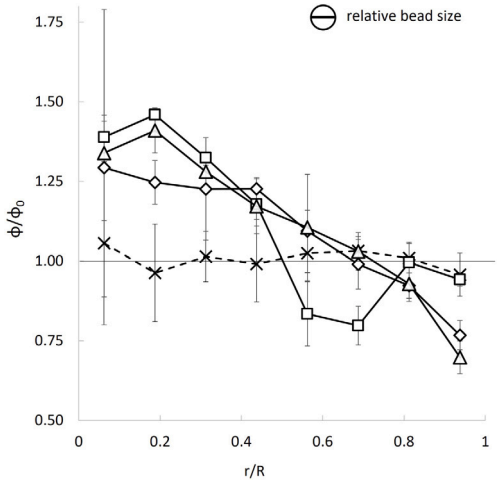

Fig. 10. Average normalized concentration profile of beads plotted as a function of normalized radial position: reference (×), 25 m flow (□), 48 m flow (⋄), and 200 m flow (△). Relative bead size is indicated.

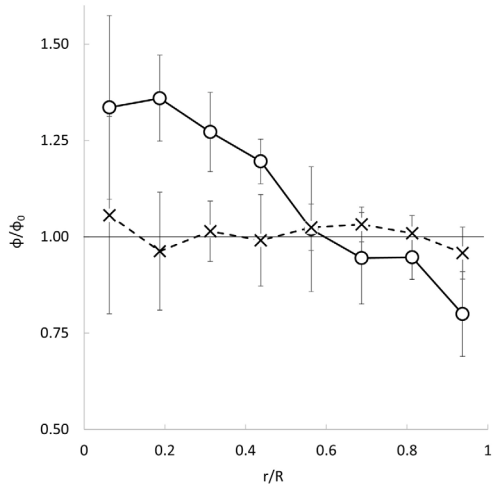

Fig. 11. Average normalized concentration profile of beads plotted as a function of normalized radial position: reference (×) and all flow samples (25 m, 48 m, 200 m) combined (○).

development length predicted for a Newtonian monodisperse suspension [18]. An extensive rheological characterization of the mortar was performed as a function of time and temperature (i.e., 20 °C and 35 °C, a temperature that may have been reached during pipe flow due to viscous dissipation). It enabled the identification of Herschel-Bulkley models, used to predict velocity profiles inside the pipe, at both temperatures. Both *dynamic* and *static* yield stresses increased with temperature, linked to cement reactivity. The *static* yield stress (paste "at rest") increased with time, gaining a factor of ca. 5 in 25 min at 20 °C, and a factor of ca. 450 during the same time at 35 °C. The analysis of the radial bead distribution was performed after the cement core had hardened, was cut and polished. All samples at all flow distances exhibited particle migration to the pipe center, reaching a bead content 35% higher, on average, than the nominal concentration. No correlation with flow distance was observed. We attributed this result to the *static* yield stress increase likely happening in the mortar present in the center flow region where limited shear occurs ("at rest"), although other effects may play a role [17,22,76].

This work shows that shear-induced particle migration occurs in cement mortars of moderate yield stress when sheared in pipe under oscillatory flow. This migration goes beyond the formation of a lubrication layer near the wall and takes place over the whole pipe cross-section. The particle motion seems to be eventually impaired by cement structuration (build-up of yield stress) that happens over time.

Further work is needed to consolidate these results. The pumping velocity should be controlled and varied to study its influence on particle migration and size of plug flow region. Mortars of various rheological properties and various reactivities (rate of structuration) should be explored as well. Measuring normal stresses on cement slurries filled with beads would be clearly valuable, although difficult. Finally, the relationship between the ability of the aggregates to migrate to the pipe center and the risk of pipe blockage during concrete pumping should be investigated through steady pumping experiments.

Declaration of competing interest

The authors declare that they have no known competing financial interests or personal relationships that could have appeared to influence the work reported in this paper.

Data availability

Data will be made available on request.

Acknowledgments

We thank Johannes Kirnbauer and Benjamin Marksteiner for their help in the design and assembly of the setup and the running of the experiments.

The authors acknowledge TU Wien Bibliothek for financial support through its Open Access Funding Programme.

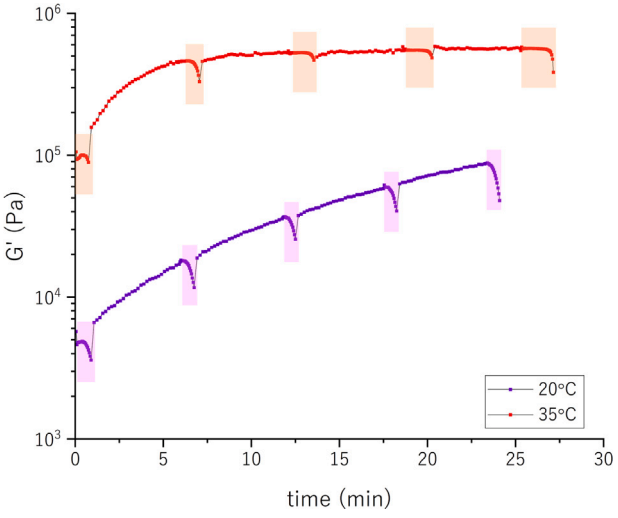

Fig. 12. Effect of temperature on the storage modulus G' of the mortar. Colored windows indicate the amplitude sweep tests.

Appendix

Time structuration of mortar. The mortar is tested at temperatures of 20 °C and 35 °C for ca. 23–27 min (inside the rheometer), as shown in Fig. 12 for two typical curves (see Section 2.2).

As already shown in Fig. 7, a rise in τ_s over time is measured at both temperatures. This result is a direct effect of the precipitation-dissolution process experienced in cement, mortar and concrete pastes. As discussed in the main manuscript, temperature accelerates this process, resulting in the development of a stiffer and stronger gel (higher G', τ_s and γ_{cr}).

References

[1] M. Choi, N. Roussel, Y. Kim, J. Kim, Lubrication layer properties during concrete pumping, Cem. Concr. Res. 45 (2013) 69–78.
[2] V. Mechtcherine, V.N. Nerella, K. Kasten, Testing pumpability of concrete using sliding pipe rheometer, Constr. Build. Mater. 53 (2014) 312–323.
[3] E. Secrieru, D. Cotardo, V. Mechtcherine, L. Lohaus, C. Schröfl, C. Begemann, Changes in concrete properties during pumping and formation of lubricating material under pressure, Cem. Concr. Res. 108 (2018) 129–139.
[4] S. Fataei, E. Secrieru, V. Mechtcherine, Experimental insights into concrete flow-regimes subject to shear-induced particle migration (SIPM) during pumping, Materials 13 (5) (2020) 1233.
[5] T. Ngo, E. Kadri, R. Bennacer, F. Cussigh, Use of tribometer to estimate interface friction and concrete boundary layer composition during the fluid concrete pumping, Constr. Build. Mater. 24 (7) (2010) 1253–1261.
[6] D. Feys, G. De Schutter, S. Fataei, N.S. Martys, V. Mechtcherine, Pumping of concrete: Understanding a common placement method with lots of challenges, Cem. Concr. Res. 154 (2022) 106720.
[7] T. Tavangar, M. Hosseinpoor, A. Yahia, K.H. Khayat, Computational investigation of concrete pipe flow: Critical review, ACI Mater. J. 118 (6) (2021).
[8] A. Karnis, S. Mason, The flow of suspensions through tubes VI. Meniscus effects, J. Colloid Interface Sci. 23 (1) (1967) 120–133.
[9] A. Ramachandran, D.T. Leighton Jr., Particle migration in concentrated suspensions undergoing squeeze flow, J. Rheol. 54 (3) (2010) 563–589.
[10] D. Kaplan, F. De Larrard, T. Sedran, Avoidance of blockages in concrete pumping process, ACI Mater. J. 102 (3) (2005) 183.
[11] R.D. Browne, P.B. Bamforth, Tests to establish concrete pumpability, J. Proc. 74 (5) (1977) 193–203.
[12] F. Gadala-Maria, A. Acrivos, Shear-induced structure in a concentrated suspension of solid spheres, J. Rheol. 24 (6) (1980) 799–814.
[13] D. Leighton, A. Acrivos, The shear-induced migration of particles in concentrated suspensions, J. Fluid Mech. 181 (1987) 415–439.
[14] C.J. Koh, P. Hookham, L.G. Leal, An experimental investigation of concentrated suspension flows in a rectangular channel, J. Fluid Mech. 266 (1994) 1–32.
[15] R. Hampton, A. Mammoli, A. Graham, N. Tetlow, S. Altobelli, Migration of particles undergoing pressure-driven flow in a circular conduit, J. Rheol. 41 (3) (1997) 621–640.
[16] V. Breedveld, D. van den Ende, A. Tripathi, A. Acrivos, The measurement of the shear-induced particle and fluid tracer diffusivities in concentrated suspensions by a novel method, J. Fluid Mech. 375 (1998) 297–318.
[17] M. Lyon, L. Leal, An experimental study of the motion of concentrated suspensions in two-dimensional channel flow. Part 1. Monodisperse systems, J. Fluid Mech. 363 (1998) 25–56.
[18] P.R. Nott, J.F. Brady, Pressure-driven flow of suspensions: Simulation and theory, J. Fluid Mech. 275 (1994) 157–199.
[19] G. Segre, A. Silberberg, Radial particle displacements in Poiseuille flow of suspensions, Nature 189 (4760) (1961) 209–210.
[20] G. Segre, A. Silberberg, Behaviour of macroscopic rigid spheres in Poiseuille flow Part 2. Experimental results and interpretation, J. Fluid Mech. 14 (1) (1962) 136–157.
[21] J.E. Butler, P.D. Majors, R.T. Bonnecaze, Observations of shear-induced particle migration for oscillatory flow of a suspension within a tube, Phys. Fluids 11 (10) (1999) 2865–2877.
[22] B. Snook, J.E. Butler, É. Guazzelli, Dynamics of shear-induced migration of spherical particles in oscillatory pipe flow, J. Fluid Mech. 786 (2016) 128–153.
[23] B. Ho, L. Leal, Migration of rigid spheres in a two-dimensional unidirectional shear flow of a second-order fluid, J. Fluid Mech. 76 (4) (1976) 783–799.
[24] N.S. Martys, W.L. George, R.P. Murphy, K.M. Weigandt, Pipe flow of sphere suspensions having a power-law-dependent fluid matrix, J. Rheol. 64 (2) (2020) 445–457.
[25] P. Huang, D. Joseph, Effects of shear thinning on migration of neutrally buoyant particles in pressure driven flow of Newtonian and viscoelastic fluids, J. Non-Newton. Fluid Mech. 90 (2–3) (2000) 159–185.
[26] M. Villone, G. D'Avino, M. Hulsen, F. Greco, P. Maffettone, Simulations of viscoelasticity-induced focusing of particles in pressure-driven micro-slit flow, J. Non-Newton. Fluid Mech. 166 (23–24) (2011) 1396–1405.
[27] J.F. Morris, F. Boulay, Curvilinear flows of noncolloidal suspensions: The role of normal stresses, J. Rheol. 43 (5) (1999) 1213–1237.
[28] M. Izadi, I. Frigaard, Squeeze cementing: Invasion of a yield stress suspension into a pore, J. Non-Newton. Fluid Mech. 298 (2021) 104681.
[29] S. Hormozi, I. Frigaard, Dispersion of solids in fracturing flows of yield stress fluids, J. Fluid Mech. 830 (2017) 93–137.
[30] I. Siqueira, P. de Souza Mendes, On the pressure-driven flow of suspensions: Particle migration in apparent yield-stress fluids, J. Non-Newton. Fluid Mech. 265 (2019) 92–98.
[31] G. D'Avino, F. Greco, P.L. Maffettone, Particle migration due to viscoelasticity of the suspending liquid and its relevance in microfluidic devices, Annu. Rev. Fluid Mech. 49 (2017) 341–360.
[32] T. Dbouk, L. Lobry, E. Lemaire, Normal stresses in concentrated non-Brownian suspensions, J. Fluid Mech. 715 (2013) 239–272.
[33] S. Garland, G. Gauthier, J. Martin, J. Morris, Normal stress measurements in sheared non-Brownian suspensions, J. Rheol. 57 (1) (2013) 71–88.
[34] F. Boyer, É. Guazzelli, O. Pouliquen, Unifying suspension and granular rheology, Phys. Rev. Lett. 107 (18) (2011) 188301.
[35] S. Dagois-Bohy, S. Hormozi, E. Guazzelli, O. Pouliquen, Rheology of dense suspensions of non-colloidal spheres in yield-stress fluids, J. Fluid Mech. 776 (2015) R2.
[36] C. Plassard, E. Lesniewska, I. Pochard, A. Nonat, Nanoscale experimental investigation of particle interactions at the origin of the cohesion of cement, Langmuir 21 (16) (2005) 7263–7270.
[37] A. Allen, R. Oberthur, D. Pearson, P. Schofield, C. Wilding, Development of the fine porosity and gel structure of hydrating cement systems, Phil. Mag. B 56 (3) (1987) 263–288.
[38] B. Jönsson, A. Nonat, C. Labbez, B. Cabane, H. Wennerström, Controlling the cohesion of cement paste, Langmuir 21 (20) (2005) 9211–9221.
[39] J.W. Bullard, H.M. Jennings, R.A. Livingston, A. Nonat, G.W. Scherer, J.S. Schweitzer, K.L. Scrivener, J.J. Thomas, Mechanisms of cement hydration, Cem. Concr. Res. 41 (12) (2011) 1208–1223.
[40] A. Goyal, I. Palaia, K. Ioannidou, F.-J. Ulm, H. Van Damme, R.J.-M. Pellenq, E. Trizac, E. Del Gado, The physics of cement cohesion, Sci. Adv. 7 (32) (2021) eabg5882.
[41] D. Hannant, J. Keating, Equipment for assessing the development of structure in fresh cement pastes by the measurement of shear modulus, Cem. Concr. Res. 15 (4) (1985) 605–612.
[42] J.E. Wallevik, Rheological properties of cement paste: Thixotropic behavior and structural breakdown, Cem. Concr. Res. 39 (1) (2009) 14–29.
[43] T. Liberto, M. Bellotto, A. Robisson, Small oscillatory rheology and cementitious particle interactions, Cem. Concr. Res. 157 (2022) 106790.
[44] B. Jönsson, H. Wennerström, A. Nonat, B. Cabane, Onset of cohesion in cement paste, Langmuir 20 (16) (2004) 6702–6709.
[45] H.M. Jennings, A model for the microstructure of calcium silicate hydrate in cement paste, Cem. Concr. Res. 30 (1) (2000) 101–116.
[46] N. Roussel, G. Ovarlez, S. Garrault, C. Brumaud, The origins of thixotropy of fresh cement pastes, Cem. Concr. Res. 42 (1) (2012) 148–157.
[47] P.F. Banfill, The rheology of fresh mortar, Mag. Concr. Res. 43 (154) (1991) 13–21.

[48] R. Flatt, I. Schober, 7 - superplasticizers and the rheology of concrete, in: N. Roussel (Ed.), Understanding the Rheology of Concrete, in: Woodhead Publishing Series in Civil and Structural Engineering, Woodhead Publishing, 2012, pp. 144–208, http://dx.doi.org/10.1533/9780857095282.2.144, URL https://www.sciencedirect.com/science/article/pii/B9780857090287500078.
[49] G. Ovarlez, F. Bertrand, P. Coussot, X. Chateau, Shear-induced sedimentation in yield stress fluids, J. Non-Newton. Fluid Mech. 177 (2012) 19–28.
[50] D. Han, R.D. Ferron, Effect of mixing method on microstructure and rheology of cement paste, Constr. Build. Mater. 93 (2015) 278–288.
[51] J. Dils, G. De Schutter, V. Boel, Influence of mixing procedure and mixer type on fresh and hardened properties of concrete: A review, Mater. Struct. 45 (11) (2012) 1673–1683.
[52] R.E. Tobin, Hydraulic theory of concrete pumping, J. Proc. 69 (8) (1972) 505–512.
[53] A. Yahia, Shear-thickening behavior of high-performance cement grouts—Influencing mix-design parameters, Cem. Concr. Res. 41 (3) (2011) 230–235.
[54] N. Roussel, Understanding the Rheology of Concrete, Woodhead Publ, Oxford, 2012.
[55] J.E. Wallevik, Thixotropic investigation on cement paste: Experimental and numerical approach, J. Non-Newton. Fluid Mech. 132 (1–3) (2005) 86–99.
[56] J.J. Thomas, H.M. Jennings, Materials of Cement Science Primer: The Science of Concrete, Tech. Rep., 2009.
[57] J. Zhang, E.A. Weissinger, S. Peethamparan, G.W. Scherer, Early hydration and setting of oil well cement, Cem. Concr. Res. 40 (7) (2010) 1023–1033.
[58] D. Feys, A. Asghari, Influence of maximum applied shear rate on the measured rheological properties of flowable cement pastes, Cem. Concr. Res. 117 (2019) 69–81.
[59] M. Gholami, A. Rashedi, N. Lenoir, D. Hautemayou, G. Ovarlez, S. Hormozi, Time-resolved 2D concentration maps in flowing suspensions using X-ray, J. Rheol. 62 (4) (2018) 955–974.
[60] M. Haist, J. Link, D. Nicia, S. Leinitz, C. Baumert, T. von Bronk, D. Cotardo, M. Eslami Pirharati, S. Fataei, H. Garrecht, et al., Interlaboratory study on rheological properties of cement pastes and reference substances: Comparability of measurements performed with different rheometers and measurement geometries, Mater. Struct. 53 (4) (2020) 1–26.
[61] S. Dhar, T. Liberto, A. Robisson, Under Preparation.
[62] N. Roussel, Steady and transient flow behaviour of fresh cement pastes, Cem. Concr. Res. 35 (9) (2005) 1656–1664.
[63] O.F. Ojeda Farías, Thixotropy of Reactive Suspensions: Application to White Portland Cement Suspensions (Ph.D. thesis), Universidad Autónoma de Nuevo León, 2019.
[64] T. Liberto, M. Le Merrer, C. Barentin, M. Bellotto, J. Colombani, Elasticity and yielding of a calcite paste: Scaling laws in a dense colloidal suspension, Soft Matter 13 (10) (2017) 2014–2023.
[65] Y. Qian, S. Kawashima, Flow onset of fresh mortars in rheometers: Contribution of paste deflocculation and sand particle migration, Cem. Concr. Res. 90 (2016) 97–103.
[66] W.Y. Shih, W.-H. Shih, I.A. Aksay, Elastic and yield behavior of strongly flocculated colloids, J. Am. Ceram. Soc. 82 (3) (1999) 616–624.
[67] R. Soto, V. Shah, Entrance flow of a yield-power law fluid, Appl. Sci. Res. 32 (1) (1976) 73–85.
[68] M. Escudier, F. Presti, Pipe flow of a thixotropic liquid, J. Non-Newton. Fluid Mech. 62 (2–3) (1996) 291–306.
[69] R. Poole, R. Chhabra, Development length requirements for fully developed laminar pipe flow of yield stress fluids, J. Fluids Eng. 132 (3) (2010).
[70] U. Sarkar, N. Biswas, Exact and limiting solutions of fluid flow for axially oscillating cylindrical pipe and annulus, SN Appl. Sci. 3 (2021) 1–14.
[71] D. Bonn, M.M. Denn, L. Berthier, T. Divoux, S. Manneville, Yield stress materials in soft condensed matter, Rev. Modern Phys. 89 (3) (2017) 035005.
[72] H.A. Barnes, The yield stress—a review or '$\pi\alpha\nu\tau\alpha\ \rho\varepsilon\iota$'—everything flows? J. Non-Newton. Fluid Mech. 81 (1–2) (1999) 133–178.
[73] D. Lootens, P. Hébraud, E. Lécolier, H. Van Damme, Gelation, shear-thinning and shear-thickening in cement slurries, Oil Gas Sci. Technol. 59 (1) (2004) 31–40.
[74] G. Bossis, P. Boustingorry, Y. Grasselli, A. Meunier, R. Morini, A. Zubarev, O. Volkova, Discontinuous shear thickening in the presence of polymers adsorbed on the surface of calcium carbonate particles, Rheol. Acta 56 (2017) 415–430.
[75] M. Han, C. Kim, M. Kim, S. Lee, Particle migration in tube flow of suspensions, J. Rheol. 43 (5) (1999) 1157–1174.
[76] A. Rashedi, M. Sarabian, M. Firouznia, D. Roberts, G. Ovarlez, S. Hormozi, Shear-induced migration and axial development of particles in channel flows of non-Brownian suspensions, AIChE J. 66 (12) (2020) e17100.